Supporting Information for "Nature of Optical Excitations in Porphyrin Crystals: A Joint Experimental and Theoretical Study"

Maurizia Palummo,[†] Luisa Raimondo,[*,‡] Conor Hogan,[*,¶,§] Claudio Goletti,[§] Silvia Trabattoni,[‡] and Adele Sassella[‡]

[†]*INFN, Dipartimento di Fisica, Università di Roma "Tor Vergata", Via della Ricerca Scientifica 1, 00133 Roma, Italy*

[‡]*Dipartimento di Scienza dei Materiali, Università degli Studi di Milano - Bicocca, Via Roberto Cozzi 55, I-20125 Milano, Italy*

[¶]*Istituto di Struttura della Materia-CNR (ISM-CNR), Via del Fosso del Cavaliere 100, 00133 Roma, Italy*

[§]*Dipartimento di Fisica, Università di Roma "Tor Vergata", Via della Ricerca Scientifica 1, 00133 Roma, Italy*

E-mail: luisa.raimondo@unimib.it; conor.hogan@ism.cnr.it

Experimental methods

Atomic force microscopy (AFM) images are collected in intermittent-contact mode in air with a Nanoscope V MultiMode (Bruker) using silicon probes (force constant 40 N/m, resonance frequency 300 kHz, tip radius 8 nm) with a resolution of 512×512 pixels.

Polarized optical absorption measurements are performed at normal incidence in the spectral range from 1.7 to 3.6 eV by using a Perkin-Elmer Lambda900 spectrometer, equipped with a depolarizer and Glan-Taylor calcite polarizers, with a light spot size of about 5 mm^2.

Plots of the molecular and crystal structure were produced with Mercury CSD 3.7.[1]

Experimental configuration in optical measurements

The absorption spectra reported in Figure 1e in the main text are collected on a 1 nm thick ZnTPP film. These spectra are a good approximation of those of a (100)-oriented ZnTPP single crystal when the light beam is normal to $(100)_{\mathrm{ZnTPP}}$ surface (thus, light propagates along the a^*_{ZnTPP} axis) and is linearly polarized with the electric field $\mathbf{E}$ parallel and orthogonal to $[001]_{\mathrm{ZnTPP}}$ (see Figure S1), notwithstanding (100)- and $(\bar{1}00)$-oriented ZnTPP crystals could coexist on KAP surface. The reason can be understood looking at Figure S2, where a view along the a^*_{ZnTPP} axis for (100)- and $(\bar{1}00)$-oriented is reported together with the directions of $\mathbf{E}$ of polarized light used for collecting spectra. The X (X') and Y (Y') directions in (100)- [$(\bar{1}00)$-] oriented ZnTPP crystals reported in Figure S2 are the orthogonal projections onto the molecular plane of the directions connecting the opposite nitrogen atoms along which the optical spectra of the isolated molecule with the conformation assumed in the crystal have been computed (see Figure 3c in the main text). At normal incidence, the projections of X and Y directions on the sample surface are connected to X' and Y' by means of a C_2 axis along c_{ZnTPP} axis. It is therefore obvious that at normal incidence no differences could be observed between the optical response of a (100)-oriented ZnTPP single crystal or a couple of crystals oriented like those reported in Figure S2 (both present in our

samples), when incident light is polarized along and perpendicularly to the c_{ZnTPP} axis. Note that the above approximation fails under any other configurations (e.g. different directions of light polarization at normal incidence or oblique incidence measurements).

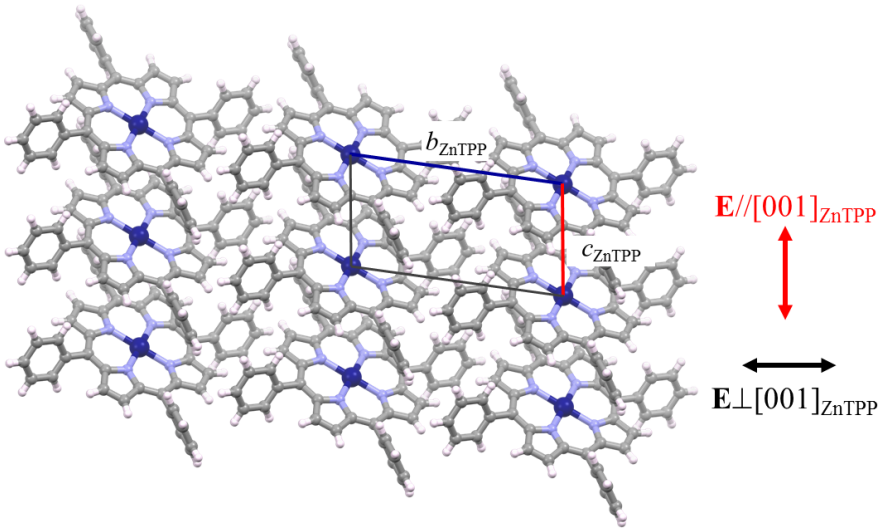

Figure S1: Sketch of the experimental configuration of the optical measurements at normal incidence. View of the crystal (one layer) along a^*_{ZnTPP}, which is also the direction of light propagation. The directions of light polarization are also reported.

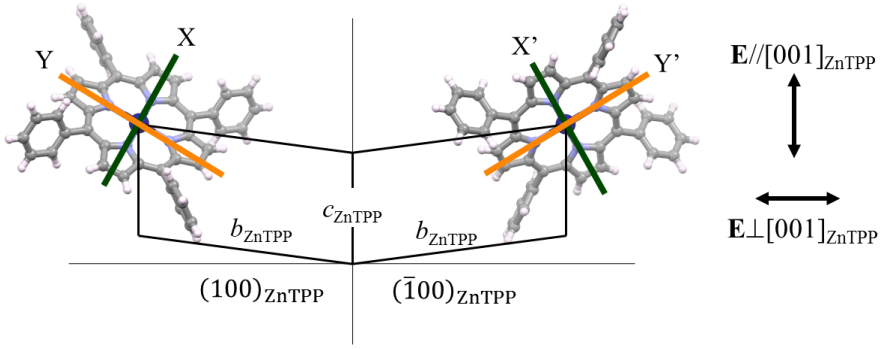

Figure S2: View along a^*_{ZnTPP} for (100)- and ($\bar{1}$00)-oriented ZnTPP crystals. For simplicity, just one unit cell is reported. X and Y axes (the same also reported in Figure 1 in the main text) are those used for computing the optical spectra of the isolated molecule with the conformation assumed in the crystal.

Theoretical Methods

The quantum-ESPRESSO package[2,3] is used for DFT simulations while all the MBPT calculations are done using Yambo.[4] We refer the reader to two previous papers on metal-free meso-tetraphenyl porphyrin (H_2TPP) where a similar theoretical/computational approach and numerical implementation have been used.[5,6]

The DFT calculations are based on plane-wave expansion and norm-conserving pseudopotentials and use the generalized gradient approximation (PBE).[7] A semi-empirical van der Waals correction[8] is added in the exchange-correlation term in order to obtain the relaxed atomic structure of the ZnTPP crystal, where as discussed in the main text, the lattice parameters are taken from experimental data. Van der Waals corrections are not used in calculations of isolated molecules. A cutoff of 70 Ry is used. Systems are modelled using periodic supercells with k-point grids of $4 \times 4 \times 4$ and Γ point only for the crystal and isolated molecule respectively. A denser grid in the π-stacking direction $3 \times 3 \times 6$ has been used to plot the excitonic wavefunctions. On top of the structural relaxation simulations, self-consistent and non-self consistent calculations are performed for the gas and solid phases. This allows us to obtain not only the occupied but also a high number of Kohn-Sham empty states needed for the excited-state simulations (up to 15 eV above the highest occupied state). To provide a good estimation of the electronic levels (bandstructure), the second step consists in carrying out GW calculations within a perturbative scheme and using the plasmon-pole approximation for the inverse dielectric matrix.[9] For the isolated molecule, due to the high computational cost, we limit the calculation to one-shot G_0W_0 approach. For the ZnTPP crystal that is the main phase of interest here, we instead apply a more expensive self-consistent GW approach by updating the energies in both G and W. This approach has been shown to improve the agreement of the energetic position of the electronic states with respect to experiment in other organic compounds, as well.[10]

The quasi-particle energies are obtained as:

$$E_i^{QP} = E_i^{KS} + \frac{1}{1-\beta_i}\langle\varphi_i^{KS}|\Sigma(E_i^{KS}) - V_{xc}|\varphi_i^{KS}\rangle, \tag{1}$$

where the index i runs over the occupied (holes h) and unoccupied (electrons e) states. $|\varphi_i^{KS}\rangle$ are the Kohn-Sham eigenfunctions, β_i is given by $\beta_i = \langle\varphi_i^{KS}|d\Sigma/dE|_{E_i^{KS}}|\varphi_i^{KS}\rangle$, i.e., the linear coefficient in the energy expansion of the self-energy Σ, which is itself the product of the Green's function G times the screened Coulomb interaction W obtained within the random phase approximation (RPA). V_{xc} is the DFT exchange-correlation potential. For the isolated molecule, a box-like cutoff in the long-range Coulomb potential is used in both GW and Bethe-Salpeter equation (BSE) calculations, in order to simulate truly isolated molecular excited states.[4,11]

The optical spectra are calculated by solving the Bethe-Salpeter equation which allows to take into account local-field and excitonic effects at the same time. By expanding the states over the Kohn-Sham basis, the solution of the BSE can be mapped onto an eigenvalue problem for the excitonic Hamiltonian.[12,13] Following similar notation as Grüning et al.,[14] we can write this matrix in the Fock space of electron-hole (eh) pairs $|eh\rangle$ and antipairs $|\overline{he}\rangle$ as:

$$H_{\text{exc}} = \begin{pmatrix} H_{\text{res}} & H_{\text{coupl}} \\ -H_{\text{coupl}}^* & -H_{\text{res}}^* \end{pmatrix}, \tag{2}$$

where the upper left (lower right) is called the resonant (antiresonant) block, is Hermitian and is defined as

$$H_{\text{res}} = (E_e^{QP} - E_h^{QP})\delta_{e,e'}\delta_{h,h'} + \langle eh|K|e'h'\rangle \tag{3}$$

where $K = W - 2\bar{v}$ is the excitonic kernel, with W and $\bar{v}$ being the screened and bare Coulomb interaction without the long-range part, and the factor 2 comes from the spin-degeneracy.[12] The coupling part $H_{\text{coupl}} = \langle eh|K|\overline{h'e'}\rangle$ is symmetric and describes the interaction between the resonant and antiresonant blocks, or in other words, between the eh pairs at positive and

negative (antipairs) energies. Here, electron-hole antipairs are denoted by $\overline{h'e'}$ while E_h^{QP}, $|h\rangle$ ($E_e^{QP}, |e\rangle$) refer to quasi-particle energies and eigenfunctions of occupied (unoccupied) states respectively. Starting from the excitonic Hamiltonian H_{exc}, it can be shown[12] that the photo-absorption cross section is proportional to

$$\begin{aligned} \sigma(\omega) &\propto \text{Im}\left(\langle 0|\vec{\xi}\cdot\vec{D}\frac{1}{(\omega - H_{\text{exc}} + iO^+)}\vec{\xi}\cdot\vec{D}|0\rangle\right) &(4)\\ &= \text{Im}\left(\langle P|\frac{1}{(\omega - H_{\text{exc}} + iO^+)}|P\rangle\right) &(5)\end{aligned}$$

where $|0\rangle$ is the ground-state wavefunction, $\vec{\xi}$ is the unit vector in the direction of the electric field of the polarized light and $\vec{D}$ is the electronic dipole, while $|P\rangle = \vec{\xi}\cdot\vec{D}|0\rangle$. Using the spectral representation, the cross-section can be rewritten in terms of excitonic eigenvalues E_λ^{exc} and eigenvectors A_λ^{eh} (which are obtained diagonalizing the excitonic matrix H^{exc}) as:

$$\begin{aligned} \sigma(\omega) &\propto \sum_\lambda |\langle\lambda|\vec{\xi}\cdot\vec{D}|0\rangle|^2\delta(\hbar\omega - E_\lambda^{exc}) &(6)\\ &= \sum_\lambda |\sum_{eh}\langle e|\vec{\xi}\cdot\vec{D}|h\rangle A_\lambda^{eh}|^2\delta(\hbar\omega - E_\lambda^{exc}) &(7)\end{aligned}$$

where $|\lambda\rangle = \sum_{eh} A_\lambda^{eh}|eh\rangle$ is the excitonic state expressed as linear combination of independent quasi-electron and holes states. It is then clear that the optical matrix elements, when local-fields and excitonic effects are taken into account, are due to a mixing of independent quasi-particle transitions mediated by the excitonic eigenvectors A_λ^{eh}.

BSE spectra: convergence, excitonic oscillator strengths, and Tamm-Dancoff approximation

Figure 3d in the main manuscript demonstrates the error induced in the peak energy position for $E\,||\,[001]_{\text{ZnTPP}}$ when the e-h states to build up the excitonic Hamiltonian (see Eq. 2 and 3) is truncated. Figure S3 illustrates the effect on the overall anisotropy: the spacing between

the peaks increases to 0.43 eV compared with 0.2 eV reported in Figure 3a at full convergence, and the lineshape and relative intensities are distinctly modified.

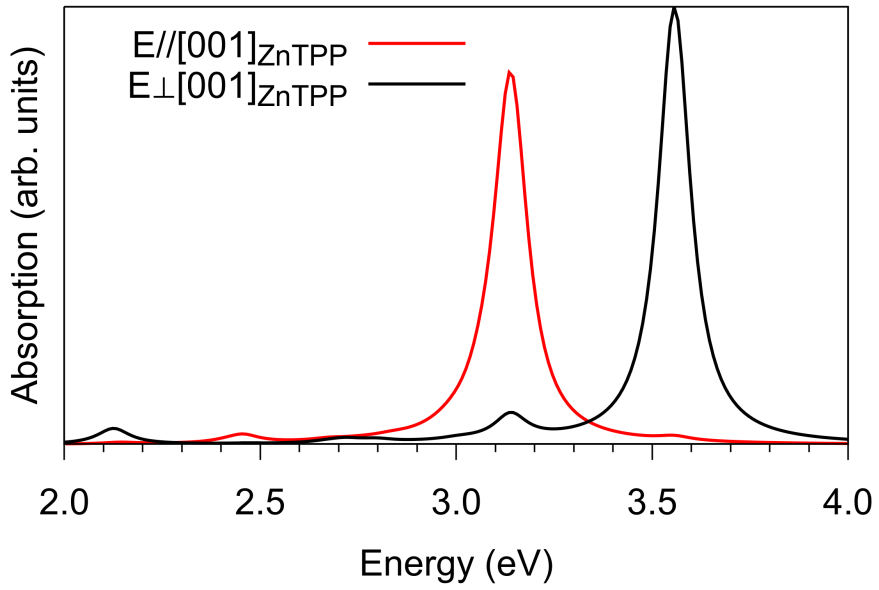

Figure S3: Absorption spectra of crystalline ZnTPP computed considering only the four a bands of Figure 2a.

Figure S4 reports the calculated oscillator strengths of all excitonic states produced by diagonalizing the excitonic matrix. It shows that several excitons, in addition to B^* and B_1^* reported in Figure 3a, are present in the B-band region. Although most of these are optically inactive at the level of theoretical approximation used in this work (i.e. where no coupling with vibrational phonon-modes is considered), they probably play a role in the exciton dynamics and transport properties of the material.

It is worth pointing out that the Tamm-Dancoff approximation (TDA), which consists in assuming that the coupling blocks are equal to zero, is generally a very good approximation for extended or periodic materials. Nevertheless, since this term is actually dominated by the unscreened Coulomb potential v, which is a measure of the inhomogeneity of the electronic density, the TDA fails for systems where the electronic density is strongly inhomogeneous, i.e. nanostructures, molecules and molecular crystals where van der Waals interactions are mainly responsible for intermolecular bonds.

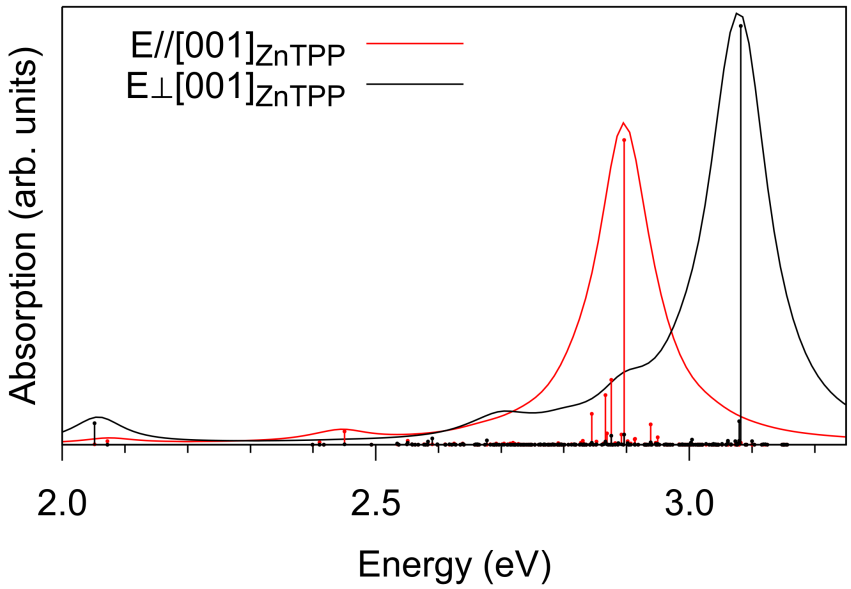

Figure S4: Absorption spectra of crystalline ZnTPP showing oscillator strengths of all excitons.

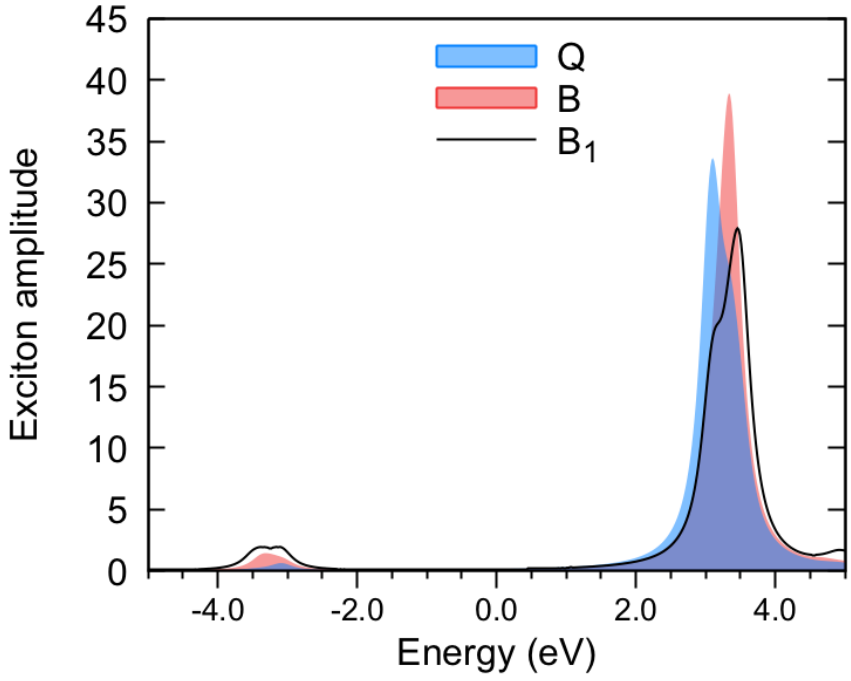

Figure S5: Exciton amplitudes $A_\lambda(\omega)$ corresponding to the Q, B and B_1 excitons.

As discussed in Ref.[14] the failure of the TDA can be quantified and understood by looking

at the amplitude functions defined as

$$A_\lambda(\omega) = \sum_{\eta=eh,\overline{he}} |\langle\eta|\lambda\rangle|^2 \delta(\omega - E_\eta). \tag{8}$$

Indeed if contributions to a given exciton λ occur also from $\overline{eh}$ antipairs, peaks at negative energies appear.

We look then at the amplitudes $A_\lambda(\omega)$ of the three main excitons Q, B, B_1, which are reported in Figure S5, where a contribution at negative energies ($\overline{he}$ antipair transitions) is clearly visible. This explains clearly the need to include the coupling parts in the excitonic Hamiltonian.

References

(1) Macrae, C. F.; Bruno, I. J.; Chisholm, J. A.; Edgington, P. R.; McCabe, P.; Pidcock, E.; Rodriguez-Monge, L.; Taylor, R.; Van De Streek, J.; Wood, P. A. Mercury CSD 2.0– New Features for the Visualization and Investigation of Crystal Structures. *J. Appl. Crystallogr.* **2008**, *41*, 466–470.

(2) Giannozzi, P.; Andreussi, O.; Brumme, T.; Bunau, O.; Buongiorno Nardelli, M.; Calandra, M.; Car, R.; Cavazzoni, C.; Ceresoli, D.; Cococcioni, M. et al. Advanced Capabilities for Materials Modelling with Quantum ESPRESSO. *J. Phys.: Condens. Matter* **2017**, *29*, 465901.

(3) Giannozzi, P.; Baroni, S.; Bonini, N.; Calandra, M.; Car, R.; Cavazzoni, C.; Ceresoli, D.; Chiarotti, G.; Cococcioni, M.; Dabo, I. et al. QUANTUM ESPRESSO: A Modular and Open-Source Software Project for Quantum Simulations of Materials. *J. Phys.: Condens. Matter* **2009**, *21*, 395502.

(4) Sangalli, D.; Ferretti, A.; Miranda, H.; Attaccalite, C.; Marri, I.; Cannuccia, E.;

Melo, P.; Marsili, M.; Paleari, F.; Marrazzo, A. et al. Many-Body Perturbation Theory Calculations Using the Yambo Code. *J. Phys.: Condens. Matter* **2019**, *31*, 325902.

(5) Palummo, M.; Hogan, C.; Sottile, F.; Bagalá, P.; Rubio, A. Ab Initio Electronic and Optical Spectra of Free-Base Porphyrins: The Role of Electronic Correlation. *J. Chem. Phys.* **2009**, *131*, 084102.

(6) Hogan, C.; Palummo, M.; Gierschner, J.; Rubio, A. Correlation Effects in the Optical Spectra of Porphyrin Oligomer Chains: Exciton Confinement and Length Dependence. *J. Chem. Phys.* **2013**, *138*, 024312.

(7) Perdew, J. P.; Burke, K.; Ernzerhof, M. Generalized Gradient Approximation Made Simple. *Phys. Rev. Lett.* **1996**, *77*, 3865–3868.

(8) Grimme, S. Semiempirical GGA-Type Density Functional Constructed with a Long-Range Dispersion Correction. *J. Comput. Chem.* **2006**, *27*, 1787–1799.

(9) Godby, R.; Schlüter, M.; Sham, L. Self-Energy Operators and Exchange-Correlation Potentials in Semiconductors. *Phys. Rev. B: Condens. Matter Mater. Phys.* **1988**, *37*, 10159–10175.

(10) Jacquemin, D.; Duchemin, I.; Blase, X. Benchmarking the Bethe-Salpeter Formalism on a Standard Organic Molecular Set. *J. Chem. Theory Comput.* **2015**, *11*, 3290–3304.

(11) Rozzi, C. A.; Varsano, D.; Marini, A.; Gross, E. K.; Rubio, A. Exact Coulomb Cutoff Technique for Supercell Calculations. *Phys. Rev. B: Condens. Matter Mater. Phys.* **2006**, *73*, 205119.

(12) Rohlfing, M.; Louie, S. G. Electron-Hole Excitations and Optical Spectra from First Principles. *Phys. Rev. B: Condens. Matter Mater. Phys.* **2000**, *62*, 4927–4944.

(13) Onida, G.; Reining, L.; Rubio, A. Electronic Excitations: Density-Functional versus Many-Body Greens-Function Approaches. *Rev. Mod. Phys.* **2002**, *74*, 601–659.

(14) Grüning, M.; Marini, A.; Gonze, X. Exciton-Plasmon States in Nanoscale Materials: Breakdown of the Tamm-Dancoff Approximation. *Nano Lett.* **2009**, *9*, 2820–2824.